Precise Relative Navigation System for a Formation Flying Astronomical Survey Telescope (FFAST)

Shinji Mitani[1], Toru Yamamoto[1], Isao Kawano[1], Takanori Iwata[1] and Hiroshi Tsunemi[2]

[1]Japan Aerospace Exploration Agency, Tsukuba 305-8505, Ibaraki, Japan ;
[2]Osaka University, Toyonaka 560-0043, Osaka, Japan

ABSTRACT

A Formation Flying Astronomical Survey Telescope (FFAST) mission that will cover much of the sky with relatively high energy X-rays has been proposed. Based on the FFAST requirements, 2 spacecrafts must be relatively controlled along 20m to an accuracy within ±10cm in the longitudinal direction and ±5mm in the lateral direction respectively. In this paper, under the consideration of the perturbation of J_2, we proposed 2 control law to achieve the required formation keeping accuracy within ±10cm and compared their performances.

FFAST の精密フォーメーションフライト制御に関する検討

巳谷真司，山元透，河野功，岩田隆敬 (JAXA)，常深博 (大阪大学)

二機の小型衛星を編隊飛行させることで望遠鏡を構成し，硬 X 線領域で広い天空をスキャン観測するミッション（FFAST）が提案されている. FFAST では，20m の距離の衛星間を望遠鏡光軸 (レンジ) 方向に ±10cm，光軸垂直方向に ±5mm の制御精度で姿勢軌道制御することを要求する. 本稿では，J_2 摂動を考慮した環境下で，レンジ方向に ±10cm の要求精度を達成する制御則について 2 案提案し，その性能を比較した.

1. INTRODUCTION

A Formation Flying Astronomical Survey Telescope (FFAST) mission that will cover much of the sky with relatively high energy X-rays is planned [1]. In the FFAST mission, a precise distance between the Mirror Spacecraft (MSC) and the Detector Spacecraft (DSC) must be maintained. The main requirement of the Formation Flying control system is to control the positioning of the center of the detector at the mirror focal point. Based on these requirements, DSC must be relatively controlled at the mirror focal point along 20 m to an accuracy of within ±10cm in the longitudinal direction and ±5mm in the lateral direction respectively. In this paper, we consider the formation keeping controller. The purpose are to obtain the controller which has less frequency of impulse maneuver in orbit around, less total delta-V, simple and robust properties. To achieve the objective, we treat the expression of relative orbital elements. This expression has the following advantage:

- Change of relative orbital elements by impulse maneuver can be expressed clearly.
- J_2 perturbation (or higher order ones) can be added easily.
- Relative acceleration (differential drag, for example) can be added.
- This expression is suited for FFAST to observe the sky area by controlling phases of relative eccentricity and inclination vector.

Shinji Mitani: E-mail: mitani.shinji@jaxa.jp, Telephone: +81-50-3362-6942

2. MODELING OF PERTURBED RELATIVE MOTION

A set of relative orbital elements $\Delta\boldsymbol{\alpha} = [\Delta a\ a\Delta e_x\ a\Delta e_y\ a\Delta i_x\ a\Delta i_y\ a\Delta u]^T$ is then defined by introducing a relative semimajor axis $\Delta a = a_2 - a_1$, a relative mean argument of latitude $\Delta u = u_2 - u_1$, a relative eccentricity vector $\Delta\boldsymbol{e} = [\Delta e_x,\ \Delta e_y]^T = [e_2\cos\omega_2 - e_1\cos\omega_1,\ e_2\sin\omega_2 - e_1\sin\omega_1]^T$, $\varphi \triangleq \arctan(\Delta e_y/\Delta e_x)$ and a relative inclination vector $\Delta\boldsymbol{i} = [\Delta i_x,\ \Delta i_y]^T = [i_2 - i_1,\ (\Omega_2 - \Omega_1)\sin i_1]^T$, $\theta \triangleq \arctan(\Delta i_y/\Delta i_x)$. One obtains after neglecting the second-order terms in the orbital elements differences and after some manipulations [2]:

$$\Delta\dot{\boldsymbol{\alpha}} = \frac{\mathrm{d}}{\mathrm{d}t}\begin{pmatrix}\Delta a\\ a\Delta e_x\\ a\Delta e_y\\ a\Delta i_x\\ a\Delta i_y\\ a\Delta u\end{pmatrix} = \begin{pmatrix}0\\ -\frac{3}{2}n\gamma(5\cos^2 i - 1)\cdot a\Delta e_y\\ \frac{3}{2}n\gamma(5\cos^2 i - 1)\cdot a\Delta e_x\\ 0\\ 3n\gamma\sin^2 i\cdot a\Delta i_x\\ -12n\gamma\sin(2i)\cdot a\Delta i_x - \frac{3}{2}n\cdot\Delta a\end{pmatrix} \tag{1}$$

The most important contribution is due to the nonuniformity of the Earth's gravity field, which induces periodic and secular perturbations of the orbit elements. In particular, if $R_\oplus$ is the equatorial radius of the Earth, J_2 is the second-order zonal coefficient of the gravity field, and

$$\gamma = \frac{J_2}{2}\left(\frac{R_\oplus}{a(1-e^2)}\right)^2 \tag{2}$$

From Eq. (1), $\Delta\boldsymbol{e}$ rotates with an angular drift rate

$$\dot{\varphi} \quad = \quad \frac{3}{2}n\gamma(5\cos^2 i - 1) \tag{3}$$

Therefore, the phase of the relative eccentricity vector $\Delta\boldsymbol{e}$ drifts during a period by an angle of

$$\delta\varphi_T \quad = \quad \dot{\varphi}\cdot T \tag{4}$$

Whereas the y component of $\Delta\boldsymbol{i}$ undergoes, during a period, a linear drift that amounts to

$$\delta i_T = 3n\gamma\sin^2 i\cdot\Delta i_x\cdot T \tag{5}$$

If $i = 31°$, then $\dot{\varphi} = 1.1838\times10^{-4}(°/\mathrm{sec})$, $\delta\varphi_T = 0.6720°$ and $\delta\theta_T = \tan(\delta i_T/\delta i^n) = 0.1334°$. Chaser drifts during a period by $a||\delta\Delta\boldsymbol{e}|| \sim 12\mathrm{cm}$, $a||\delta\Delta\boldsymbol{i}|| \sim 4\mathrm{cm}$ and $a\delta\Delta u \sim 5.4\mathrm{cm}$, which cannot be neglected compared with FFAST requirement accuracy. Finally, the expression for $\delta\Delta\boldsymbol{\alpha}$ by the chaser velocity increment vector $\delta\boldsymbol{v} = [\delta v_R,\ \delta v_T,\ \delta_N]^T$ is

$$\delta\Delta\boldsymbol{\alpha}(t) = \begin{bmatrix}\delta\Delta a\\ a\delta\Delta e_x\\ a\delta\Delta e_y\\ a\delta\Delta i_x\\ a\delta\Delta i_y\\ a\delta\Delta u\end{bmatrix} = B(t)\begin{bmatrix}\delta v_R\\ \delta v_T\\ \delta v_N\end{bmatrix} \triangleq \frac{1}{n}\begin{bmatrix}0 & 2 & 0\\ \sin u & 2\cos u & 0\\ -\cos u & 2\sin u & 0\\ 0 & 0 & \cos u\\ 0 & 0 & \sin u\\ -2 & 0 & -\sin u\cdot\cot i\end{bmatrix}\begin{bmatrix}\delta v_R\\ \delta v_T\\ \delta v_N\end{bmatrix} \tag{6}$$

where δv_R, δv_T and δv_N denote the components of the chaser velocity increment executed at time t.

3. CONTROLLER DESIGN

3.1 Proposed controller 1: Quasi-optimal controller to suppress the fuel consumption

The state transition matrix can be expressed using Eq. (1):

$$\Phi_{\Delta\alpha}(t_1,t_0) = \begin{bmatrix}1 & 0 & 0 & 0 & 0 & 0\\ 0 & \cos\Delta\varphi & -\sin\Delta\varphi & 0 & 0 & 0\\ 0 & \sin\Delta\varphi & \cos\Delta\varphi & 0 & 0 & 0\\ 0 & 0 & 0 & 1 & 0 & 0\\ 0 & 0 & 0 & \alpha_\gamma\Delta u & 1 & 0\\ -1.5\Delta u & 0 & 0 & \beta_\gamma\Delta u & 0 & 1\end{bmatrix} \tag{7}$$

where, $\Delta\varphi = \dot{\varphi}\Delta t,\ \Delta u = u(t_1) - u(t_0),\ \Delta t = t_1 - t_0,\ \alpha_\gamma = 3\gamma\sin^2 i,\ \beta_\gamma = -12\gamma\sin(2i)$. Using this matrix, propagation of $\Delta\boldsymbol{\alpha}$ from t_0 to t_1 is

$$\Delta\boldsymbol{\alpha}(t_1) = \Phi(t_1, t_0)\Delta\boldsymbol{\alpha}(t_0) \tag{8}$$

We now define the control forces exerted on the chaser spacecraft $\delta\boldsymbol{v} = [\delta v_R\ \delta v_T\ \delta v_N]^T$ and assume that they are given impulsive forces of magnitude $\delta\boldsymbol{v}_i$ at time $t = \tau_i$ $(i = 1, 2, \cdots, N)$. Then $\delta\boldsymbol{v}$ is expressed as

$$\delta\boldsymbol{v} = \sum_{i=1}^{N} \delta\boldsymbol{v}_i \delta(t - \tau_i) \tag{9}$$

Using Eq. (6) and based on the solutions obtained Eq. (8), we express the state $\Delta\boldsymbol{\alpha}$ at $t = T$ as follows

$$\Delta\boldsymbol{\alpha}(T) = \Phi_{\Delta\alpha}(T, 0)\Delta\boldsymbol{\alpha}(0) + \sum_{i=1}^{N} \Psi_{\Delta\alpha}(T, \tau_i)\delta\boldsymbol{v}_i \tag{10}$$

$$\Psi_{\Delta\alpha}(t_1, t_0) = \Phi_{\Delta\alpha}(t_1, t_0)B(t_0) \tag{11}$$

This equation reduces to

$$\Delta\tilde{\boldsymbol{\alpha}}(T) = \boldsymbol{\Psi}_{\Delta\alpha}\delta\boldsymbol{V} \tag{12}$$

where

$$\Delta\tilde{\boldsymbol{\alpha}} \triangleq \Delta\boldsymbol{\alpha} - \Phi_{\Delta\alpha}(T, 0)\Delta\boldsymbol{\alpha}(0) \tag{13}$$

$$\boldsymbol{\Psi}_{\Delta\alpha} \triangleq [\Psi_{\Delta\alpha}(T, \tau_1)\ \cdots\ \Psi_{\Delta\alpha}(T, \tau_N)] \tag{14}$$

$$\delta\boldsymbol{V} \triangleq [\delta\boldsymbol{v}_1^T\ \cdots\ \delta\boldsymbol{v}_N^T]^T \tag{15}$$

When focusing on the solution that minimizes the L_2-norm (Euclid norm) $||\delta\boldsymbol{V}||_2$, the solution is expressed on the assumption that $N \geq 2$ and $\boldsymbol{\Psi}_{\Delta\alpha}$ is a full-rank matrix:

$$\delta\boldsymbol{V} = \boldsymbol{\Psi}_{\Delta\alpha}^T(\boldsymbol{\Psi}_{\Delta\alpha}\boldsymbol{\Psi}_{\Delta\alpha}^T)^{-1}\Delta\tilde{\boldsymbol{\alpha}}(T) \tag{16}$$

Equation becomes continuous controller by taking the limit of $\Delta\tau \to 0$ $(N \to \infty)$, then

$$\Delta\boldsymbol{\alpha}(t) = \Phi_{\Delta\alpha}(t, 0)\Delta\boldsymbol{\alpha}(0) + C(t, T)C^{-1}(T, T)\Delta\tilde{\boldsymbol{\alpha}} \tag{17}$$

$$C(t, T) = \int_0^T \Psi_{\Delta\alpha}(t - \tau)\Psi_{\Delta\alpha}^T(T - \tau)\mathrm{d}\tau \tag{18}$$

Since $C(t, T)$ can be obtained analytically, the solution of the above equation is also obtained at each time [3].

3.2 Proposed controller 2: Target guidance controller

Define $\bar{\boldsymbol{X}} \triangleq [x\ y\ z\ \dot{x}/n\ \dot{y}/n\ \dot{z}/n]^T$. Transformation from $\Delta\boldsymbol{\alpha}$ to $\bar{\boldsymbol{X}}$ is [2]

$$\bar{\boldsymbol{X}}(t) = \Gamma(u(t))\Delta\boldsymbol{\alpha}(t) \tag{19}$$

where

$$\Gamma(u(t)) = \begin{bmatrix} 1 & -\cos u & -\sin u & 0 & 0 & 0 \\ 0 & 2\sin u & -2\cos u & 0 & \cot i & 1 \\ 0 & 0 & 0 & \sin u & -\cos u & 0 \\ 0 & \sin u & -\cos u & 0 & 0 & 0 \\ -\frac{3}{2} & 2\cos u & 2\sin u & 0 & 0 & 0 \\ 0 & 0 & 0 & \cos u & \sin u & 0 \end{bmatrix} \tag{20}$$

Using Eq. (8),

$$\bar{\boldsymbol{X}}(t_1) = \Gamma(t_1)\Phi_{\Delta\alpha}(t_1,t_0)\Gamma^{-1}(t_0)\bar{\boldsymbol{X}}(t_0) \triangleq \Phi_X(t_1,t_0)\bar{\boldsymbol{X}}(t_0) \tag{21}$$

Submatrices of $\Phi_X(t_1,t_0) \triangleq [\phi_{11}\ \phi_{12};\ \phi_{21}\ \phi_{22}]$ are

$$\begin{aligned}
\phi_{11} &= \begin{bmatrix} 4-3\cos[\Delta(u-\varphi)] & 0 & 0 \\ 6(\sin[\Delta(u-\varphi)]-\Delta u) & 1 & (\alpha_\gamma\cot i+\beta_\gamma)\sin u_0\Delta u \\ 0 & 0 & \cos\Delta u-\alpha_\gamma\sin u_0\cos u_1\Delta u \end{bmatrix} \\
\phi_{12} &= \begin{bmatrix} \sin[\Delta(u-\varphi)] & 2(1-\cos[\Delta(u-\varphi)]) & 0 \\ -2(1-\cos[\Delta(u-\varphi)]) & 4\sin[\Delta(u-\varphi)]-3\Delta u & (\alpha_\gamma\cot i+\beta_\gamma)\cos u_0\Delta u \\ 0 & 0 & \sin\Delta u-\alpha_\gamma\cos u_0\cos u_1\Delta u \end{bmatrix} \\
\phi_{21} &= \begin{bmatrix} 3\sin[\Delta(u-\varphi)] & 0 & 0 \\ -6(1-\cos[\Delta(u-\varphi)]) & 0 & 0 \\ 0 & 0 & -\sin\Delta u+\alpha_\gamma\sin u_0\sin u_1\Delta u \end{bmatrix} \\
\phi_{22} &= \begin{bmatrix} \cos[\Delta(u-\varphi)] & 2\sin[\Delta(u-\varphi)] & 0 \\ -2\sin[\Delta(u-\varphi)] & 4\cos[\Delta(u-\varphi)]-3 & 0 \\ 0 & 0 & \cos\Delta u+\alpha_\gamma\cos u_0\sin u_1\Delta u \end{bmatrix}
\end{aligned}$$

If there is no effect of J_2 perturbation (i.e., $J_2 = 0$), then $\Delta\varphi = \alpha_\gamma = \beta_\gamma = 0$ and matrix Φ_X yields H-C-W matrix. Once propagation matrix Φ_X obtained, the velocity change $\delta\boldsymbol{v}$ is derived to move back to the reference relative orbit $\boldsymbol{r}_t(t)$:

$$\delta\boldsymbol{v}_i = n\phi_{12}^{-1}(t_{i+1},t_i)[\boldsymbol{r}_t(t_{i+1}) - \phi_{11}(t_{i+1},t_i)\boldsymbol{r}_t(t_i)] - \boldsymbol{v}^-(t_i) \tag{22}$$

Controlled relative orbit during $\tau_i \le t < \tau_{i+1} = \tau_i + \Delta\tau$ are

$$\bar{\boldsymbol{X}}(t) = \Phi_X(t,\tau_i)\bar{\boldsymbol{X}}(\tau_i) + \Psi_X(t,\tau_i)\delta\boldsymbol{v}_i \tag{23}$$

$$\Psi_X(t_1,t_0) = \Phi_X(t_1,t_0)B(t_0) \tag{24}$$

When taking the limit of $\Delta\tau \to 0$ ($N \to \infty$), then

$$\lim_{\Delta\tau\to 0} ||\boldsymbol{r}(t) - \boldsymbol{r}_t(t)||_2 = 0 \tag{25}$$

4. SIMULATION RESULT

We compare the proposed two controllers' performance. The setting parameters are h=500km, $i = 31°$, T=5677sec. Reference relative orbital elements is set to $\Delta\boldsymbol{\alpha}_t = [0,\ (0,\ 10),\ (17.32,\ 0),\ 0]^T$ (m) and $\bar{\boldsymbol{X}}_t(t) = [\boldsymbol{r}_t,\ \bar{\boldsymbol{v}}_t]^T = \Gamma(t)\Delta\boldsymbol{\alpha}_t$. Figure 1 shows relative range profile during 3 orbit periods ($3T = 17031$sec) when varying frequency of impulsive maneuver per 1 period. As seen in Fig. 1 Left, L_2-norm suppression controller (proposed controller 1) maintains relative range within 20 ± 0.1m but it seems difficult to maintain relative range within 20 ± 0.05m, even if frequency of impulsive maneuver become larger. On the other hand, target guidance controller (proposed controller 2) maintains relative range within 20 ± 0.05m (shown in Fig.1 Right). Moreover, when frequency of impulsive maneuver becomes larger, then the range error become smaller.

Figure 2 Left shows max range error when varying number of impulsive maneuver per 1 period. When using proposed controller 1, max range error is minimized with 5∼8 maneuvers per 1 period. When using proposed controller 2, max range error approaches to 0 if frequency of maneuver become larger. Figure 2 Right shows consuming ΔV when varying number of impulsive maneuver per 1 period. Proposed controller 1 is superior to proposed controller 2 in terms of ΔV performance.

Figure 3 and 4 show relative orbital elements for proposed controller 1 (with 3 and 100 maneuvers per around, respectively). Likewise, Fig. 5 and 6 show relative orbital elements for proposed controller 2.

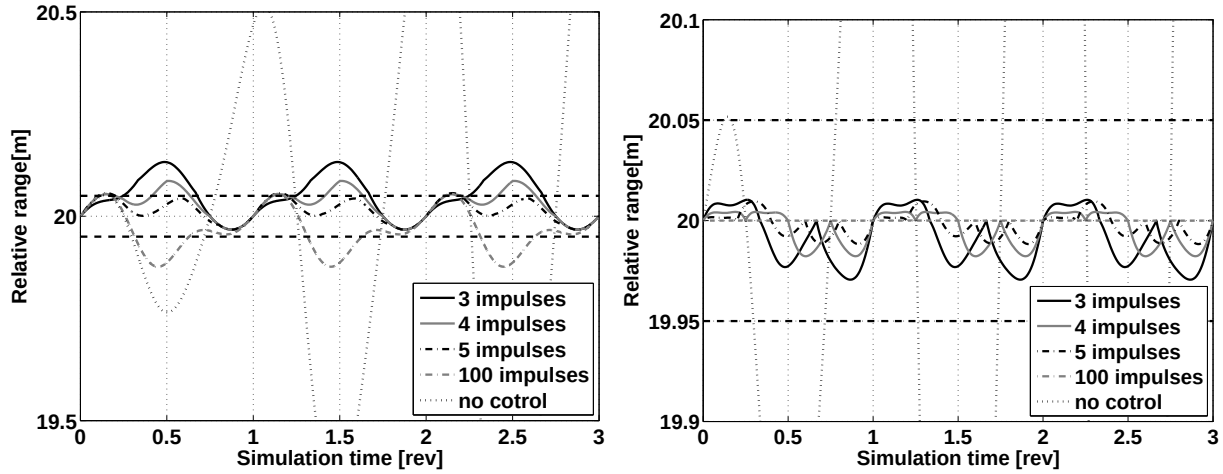

Figure 1. Relative range profile over 3 rounds (Left: L_2-norm suppression controller, Right: Target guidance controller).

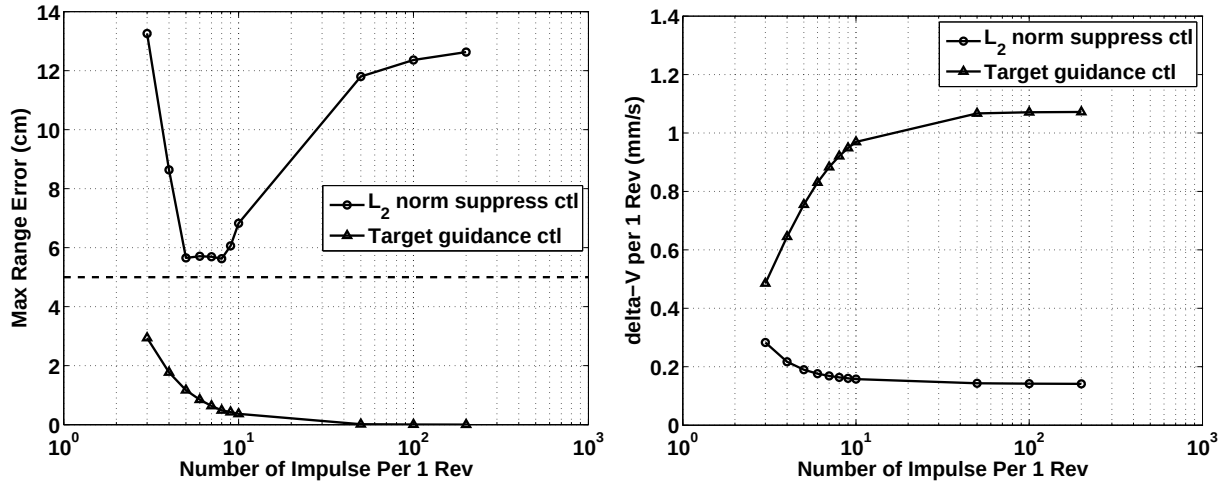

Figure 2. Comparison between 2 proposed controller performances (Left: Max range error, Right: Consuming ΔV).

5. CONCLUDING REMARKS

In this paper, we studied how to control the orientation range error within ±5cm, considering the J_2 perturbation. Using the L_2-norm suppression controller, the amount of fuel consumption can be reduced to less than 0.2mm/s. But it is difficult to keep the required accuracy range even if frequency of impulse become large. Using guidance controller to move back to the reference orbit at regular intervals, the required accuracy can be satisfied with only 3 impulse per 1 period. Moreover, it is possible to decrease the range error monotonically with increasing the number of impulse whereas the amount of fuel consumption increase. Therefore it is necessary to set the number of impulse per 1 period taking into account the amount of fuel consumption.

REFERENCES

[1] Tsunemi, H., et al., "High Energy X-Ray Sky Observation by the Formation Flight All Sky Telescope", Trans. JSASS Aerospace Tech. Japan, vol. 8, No. ists27, 2010.

[2] Ardaesens, J., D'Amico, S., "Spaceborne Autonomous Relative Control System for Dual Satellite Formations", Journal of Guidance, Control, and Dynamics, Vol. 32, No. 6, Nov-Dec 2009, pp. 1859-1870.

[3] Yamada, K., Yoshikawa, S. and Nishiyama, T., "On Relative Position Control between Two Spacecraft", Workshop on Astrodynamics and Flight Mechanics, 2003.

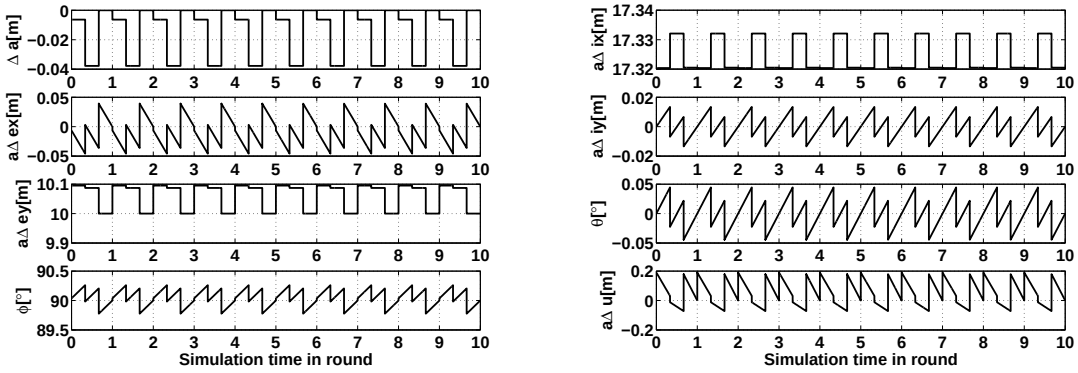

Figure 3. Relative orbital elements for L2 norm suppression controller (3 impulse maneuvers/rev).

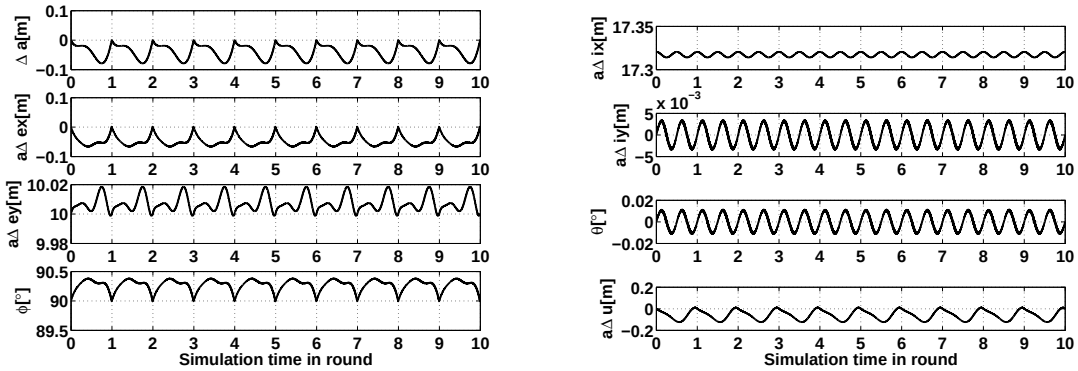

Figure 4. Relative orbital elements for L2 norm suppression controller (100 impulse maneuvers/rev).

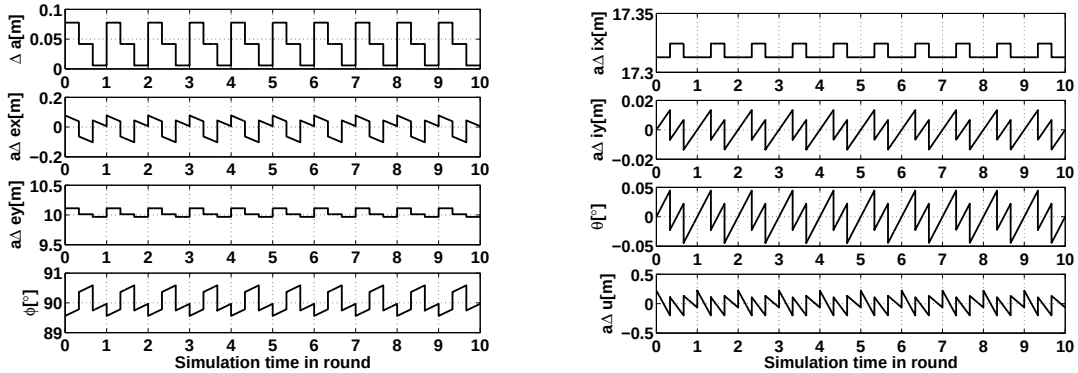

Figure 5. Relative orbital elements for target guidance controller (3 impulse maneuvers/rev).

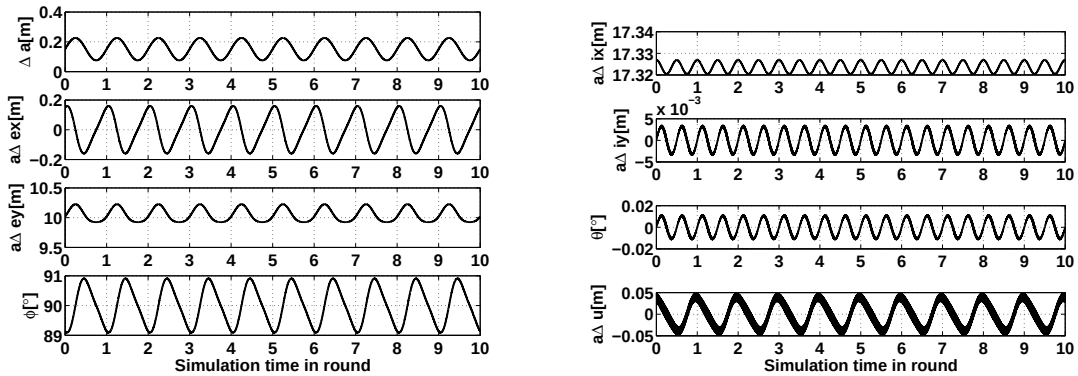

Figure 6. Relative orbital elements for target guidance controller (100 impulse maneuvers/rev).